INTERNATIONAL JOURNAL FOR NUMERICAL AND ANALYTICAL METHODS IN GEOMECHANICS
Int. J. Numer. Anal. Meth. Geomech., **23**, 1195–1214 (1999)

BOUNDARY ELEMENT ANALYSIS OF GEOMECHANICAL FRACTURE

A. J. WILDE[1] AND M. H. ALIABADI[2]*

[1] *GEC-Marconi, Surrey, GU16 SPE, UK*
[2] *Department of Engineering, Queen Mary College, University of London, Mile End, London E1 4NS, UK*

SUMMARY

In this paper, a single-region BEM formulation for the three-dimensional analysis of fractures in geomechanics is developed. The technique allows the use of continuous elements in the discretization of the crack surfaces. Intially, an example from earthquake control theory is solved to demonstrated the validity of the technique for partially loaded crack surfaces. The method is then extended to deal with contact between crack surfaces by the incorporation of spring constraints. This allows two futher applications to be studied, one from hydraulic fracture and the other involving extraction of an ore seam. Copyright © 1999 John Wiley & Sons, Ltd.

1. INTRODUCTION

Boundary Element Methods (BEM) have enjoyed considerable success in the area of geomechanics,[1–2] arising from their ability to implicitly satisfy various far-field boundary conditions in media of infinite or semi-infinite extent. This is particularly true for linear, homogenous materials although various inhomogeneties in the material have been successfully treated. A characteristic of rock material is the presence of joints and faults, along which discontinuous behaviour occurs, requiring the implementation of special techniques. One such technique, extensively used elsewhere, is the Dual Boundary Element Method (DBEM)[3–6] which has the advantages associated with boundary element techniques, in a single region formulation. Comprehensive reviews of the application of BEM to fracture mechanics and the DBEM methods are presented by References 7 and 8 respectively.

The boundary element method in elastostatics requires evaluation of singular integral equations. Problems involving no degenerate volumes or areas may be solved using a single equation known as the displacement Boundary Integral Euation (BIE). This equation contains both weakly and strongly singular integrals. The calculation of the weakly singular integral presents no problems, and direct calculation of the strongly singular integral may, by use of the rigid body condition, be avoided all together.

However, if the body under analysis contains a crack, the application of the standard method leads to mathematical degeneration in the numerical formulation, since the two surfaces of the

*Correspondence to: M. H. Aliabadi, Department of Engineering, Queen Mary College, University of London, Mile End, London E1 4NS, UK

CCC 0363–9061/99/121195–20$17.50

Received 17 December 1997
Revised 23 September 1998

crack may be considered coplanar. To avoid this problem, a second equation, known as the traction boundary integral equation (TBIE) is applied to a single surface of the crack, and the BIE is used on all other surfaces. This technique is the basis for the Dual boundary element method as proposed by Portela *et al.*,[4] and developed for three-dimensional problems by Mi and Aliabadi.[5]

The kernels in the TBIE are linear combinations of the derivatives of the kernels in the BIE and hence their singularity will be one order higher. Direct evaluation of these singular integrals cannot be avoided in crack problems (see Reference 9), which means that the use of Cauchy and Hadamard interpretations of the singular integrals, together with certain assumptions about the continuity of the displacements and tractions are necessary. The most general strategy employed to satisfy these requirements involves the use of quadratic discontinuous elements. These elements ensure, by moving the source point to the interior, that wherever the TBIE is collocated the interpolation of the field variables is infinitely smooth. However, using these elements for large three dimensional crack problems the number of degrees of freedom of the solution matrix may be large.

In general, continuous elements are more convenient to use and give rise to smaller solution matrices. These benefits mean it has been important to design a numerical scheme for solution of the TBIE using continuous elements. One such scheme is that proposed by Young,[10] where an indirect strategy is employed involving the analysis of the so-called boundary integral equation for displacement derivatives (DDBIE) which is then converted to the TBIE via Hooke's Law. A similar procedure was applied to crack problems in geomechanics by Wilde and Aliabadi,[11] and to the evaluation of boundary stresses by the same authors.[12] In this work, which can be considered an extension of Reference 11, the incorporation of the continuity conditions into a special interpolation of the field variables arising from this scheme is explored. The procedure leading to the full DBEM formulation is briefly reviewed, and an example from earthquake control theory is used to verify the technique for the previously untested problem of a partially loaded crack. The method is then extended to deal with contact between crack surfaces by the incorporation of spring constraints between opposing nodes on the upper and lower crack surfaces nodes. The inclusion of these constraints into the solution matrix is then demonstrated. This allows two further applications to be studied, one from hydraulic fracture and the other involving extraction of an ore seam.

2. THE DDBIE AND CONTINUITY REQUIREMENTS

Somigliana's Identity at a point $\mathbf{x}'$ interior to a surface Γ bounding a homogeneous, isotropic, linear elastic solid V is given by

$$u_j(\mathbf{x}') + \int_\Gamma \{T_{ij}(\mathbf{x}, \mathbf{x}')\, u_i(\mathbf{x}) - U_{ij}(\mathbf{x}, \mathbf{x}')\, t_i(\mathbf{x})\}\, \mathrm{d}\Gamma(\mathbf{x}) = 0 \tag{1}$$

where T_{ij} and U_{ij} are the Kelvin fundamental solutions (see Appendix I).

The derivative of (1) with respect to the interior source point coordinate $\mathbf{x}'_k$ is given by

$$u_{j,k}(\mathbf{x}') + \int_\Gamma \{T_{ijk}(\mathbf{x}, \mathbf{x}')\, u_i(\mathbf{x}) - U_{ijk}(\mathbf{x}, \mathbf{x}')\, t_i(\mathbf{x})\}\, \mathrm{d}\Gamma(\mathbf{x}) = 0 \tag{2}$$

where T_{ijk} and U_{ijk} are given as in Appendix I. When the source point in equation (2) is taken to the boundary the resultant equation is known as the displacement derivative boundary integral equation (DDBIE). An alternative approach is to start with the point $\mathbf{x}'$ on the boundary and augment the surface around it with an infinitesimal sphere (see Appendix II), so that $\mathbf{x}'$ is included, and consider the limit $\varepsilon \to 0$. This gives,

$$c_{ijk}\, u'_{i,l} = \oint\!\!\!\!\!\!= \int_\Gamma U_{ijk}(\mathbf{x}, \mathbf{x}')\, t_i(\mathbf{x})\, \mathrm{d}\Gamma - \oint\!\!\!\!\!\!- \int_\Gamma T_{ijk}(\mathbf{x}, \mathbf{x}')\, u_i(\mathbf{x})\, \mathrm{d}\Gamma \\ - d_{ijk}\, u'_i + \alpha_{jk} \log \varepsilon + \beta_{jk}\, \varepsilon^{-1} \tag{3}$$

where the terms c_{iljk} and d_{ijk} are $O(1)$, and $\oint\!\!\!\!\!\!=$ and $\oint\!\!\!\!\!\!-$ denote the Hadamard and Cauchy principal values, respectively. The $\log \varepsilon$ term comes solely from the integral over the original area that is exterior to the sphere, both free terms come from the integral over the sphere, and the ε^{-1} terms comes from the integrals over both these areas. The presence of the second free term d_{ijk} has been overlooked in previous analyses, possibly because it only arises when there is a jump in the boundary curvature at the source point. Recently, Mantic and Paris,[4] Guiggiani[3] and Young[10] have demonstrated the existence of this free term for hypersingular boundary integral equations.

Conventionally, the use of finite part integrals has required a level of continuity to be imposed on the assumed form of displacement and tractions fields namely that the traction and displacement derivative should be Hölder continuous. This is a stringent condition and there has been much discussion (see, for example References 15 and 16) about the circumstances under which this condition may be weakened. Sladek and Sladek[17] have also investigated these continuity conditions for hypersingular kernels for $C^{(0)}$ and $C^{(1)}$ continuous elements and, also for Overhauser elements. By the definition of finite-part integrals all the singular terms appearing in (3) must cancel if the assumed form for traction and displacement derivative are Hölder continuous. The focus in this work is to ensure this condition can be achieved without violating the physical properties of linear elastic theory. If the field variables are approximated with piecewise continuous interpolations there will, in general, be a different set of displacement derivatives for each element adjoining a node. The first stage is therefore to replace these separate displacement derivatives with a unique displacement derivative. The second stage is to combine the generalized Hooke's Law with, the traction–stress relation at the source point to obtain,

$$t'_i = n'_j\, E_{ijkl}\, u'_{k,l} \tag{4}$$

where n'_j denote the components of the outward normal and

$$E_{ijkl} = \frac{E}{2(1+\nu)} \left(\delta_{ik}\, \delta_{jl} + \delta_{ik}\, \delta_{jl} + \frac{2\nu}{1-2\nu}\, \delta_{ij}\, \delta_{kl}\right) \tag{5}$$

Equation (4) provides a basis for the unique displacement derivative at the source point, i.e. one that is consistent with the tractions at the source point.

In summary, providing the displacement derivative is $C^{(0)}$ continuous and the traction is related to the displacements derivatives at the source point by equation (4) then all singular terms will cancel, no linear elastic properties are violated and the DDBIE can be applied at any point on the surface. It is sufficient to assume simple continuity as opposed to Hölder continuity (generally Hölder is more restrictive) since the interpolations are based on well-behaved polynomial functions.

3. SPECIAL INTERPOLATION

The standard interpolation scheme is given in terms of the nodal displacements, tractions, and shape functions by

$$u_i(\mathbf{x}) \equiv \sum_{\alpha} u_i^{\alpha} M^{\alpha}(\boldsymbol{\xi}) \tag{6}$$

$$t_i(\mathbf{x}) \equiv \sum_{\alpha} t_i^{\alpha} M^{\alpha}(\boldsymbol{\xi}) \tag{7}$$

where $\boldsymbol{\xi}$ is the local position vector on the element.

This scheme is satisfactory for elements not containing the source point, since the continuity conditions prescribed in the previous section are only relevant in the vicinity of the source point.

Inspection of the standard interpolation for continuous elements reveals that a unique value of displacement is assigned to nodes shared between elements and thus u_i' is implicitly continuous. However, the stronger continuity condition on the displacement derivative and the relation (4) are not, in general, satisfied by the standard interpolation for singular elements, so a new interpolation is prescribed in which these requirements are embedded.

Reverting to the co-ordinates defined on the tangent plane for each element, the shape function $M^{\alpha}(\boldsymbol{\xi})$ can be expanded in terms of the polar radius ρ about the local source point $\boldsymbol{\xi}'$,

$$M^{\alpha}(\boldsymbol{\xi}) = M^{\alpha}(\boldsymbol{\xi}') + M^{\alpha}_{,j}(\boldsymbol{\xi}')\,\rho_j + O(\rho^2) \tag{8}$$

where the subscript '$,j$' denotes differentiation with respect to ρ_j.

Substituting into equation (6), gives

$$\begin{aligned} u_i(\mathbf{x}) &= \sum_{\alpha} u_i^{\alpha} M^{\alpha}(\boldsymbol{\xi}') + \sum_{\alpha} u_i^{\alpha} M^{\alpha}_{,j}(\boldsymbol{\xi}')\,\rho_j \\ &= u_i' + \bar{u}_{i,j}'\,\rho_j \end{aligned} \tag{9}$$

The $\bar{u}_{i,j}'$ are displacement derivatives at the source point due to the standard interpolation. They involve derivatives of shape functions, and as such are element dependent, i.e. not single-valued. The continuity requirement dictates that they are unique, thus the special interpolation scheme replaces $\bar{u}_{i,j}'$ with unique values of the displacement derivative $\tilde{u}_{i,j}'$ which are consistent with equation (4). Removing $\bar{u}_{i,j}'$ and adding $\tilde{u}_{i,j}'$ in equation (6) gives,

$$\tilde{u}_i(\boldsymbol{\xi}) = \bar{u}_i(\boldsymbol{\xi}) - \bar{u}_{i,j}'\,\rho_j + \tilde{u}_{i,j}'\,\rho_j \tag{10}$$

In order to restrict this effect to the region surrounding the source point an additional localizing function $L(\boldsymbol{\xi})$ is included such that,

$$\tilde{u}_i(\boldsymbol{\xi}) = \bar{u}_i(\boldsymbol{\xi}) + [\tilde{u}_{i,j}'\,\rho_j - \bar{u}_{i,j}'\,\rho_j]L(\boldsymbol{\xi}) \tag{11}$$

It only remains to ensure that the traction at the source point t_i' is consistent with $\tilde{u}_{i,j}'$. This is done by subtracting the traction term due to the standard interpolation at the source point, $\bar{t}_i'$, and adding in a new term, $\tilde{t}_i(\boldsymbol{\xi}')$, based on equation (4),

$$\begin{aligned} \tilde{t}_i(\boldsymbol{\xi}) &\equiv \bar{t}_i(\boldsymbol{\xi}) - \bar{t}_i(\boldsymbol{\xi}') + \tilde{t}_i(\boldsymbol{\xi}') \\ &= \bar{t}_i(\xi) - \bar{t}_i(\boldsymbol{\xi}') + E_{ijkl}\,n_j'\,\tilde{u}_{k,l}' \end{aligned} \tag{12}$$

Again, the effect should be restricted to the vicinity of the source point, so the localizing function $L(\xi)$ is included to give,

$$\tilde{t}_i(\xi) = \bar{t}_i(\xi) + [E_{ijkl}\, n'_j\, \tilde{u}'_{k,l} - \bar{t}_i(\xi')]L(\xi) \tag{13}$$

or

$$\tilde{t}_i(\xi) = \sum_{\alpha} t_i^{\alpha}[M^{\alpha}(\xi) - L(\xi)\delta_{\alpha\alpha'}] + E_{ijkl}\, n'_j\, \tilde{u}'_{k,l}\, L(\xi) \tag{14}$$

In summary, the special interpolation, comprising of equations (11) and (14), is required when continuous elements containing the source point are used. In all other cases the standard interpolation is satisfactory.

4. NUMERICAL IMPLEMENTATION

4.1. Conversion to the TBIE

When the special interpolation is included and the coefficients of $u'_{i,l}$ are collected together into a single term, the DDBIE can be written as

$$\begin{aligned} \hat{c}_{iljk}\, u'_{i,l} = &- d_{ijk}\, u'_i + \int_{\Gamma_R} U_{ijk}(\mathbf{x}, \mathbf{x}')\, \bar{t}_i(\mathbf{x})\, \mathrm{d}\Gamma \\ &+ \int_{\Gamma_S} U_{ijk}(\mathbf{x}, \mathbf{x}') \sum_{\alpha} t_i^{\alpha}[M^{\alpha}(\xi) - L(\xi)\delta_{\alpha\alpha'}]\, \mathrm{d}\Gamma \\ &- \int_{\Gamma_R} T_{ijk}(\mathbf{x}, \mathbf{x}')\, \bar{u}_i(\mathbf{x})\, \mathrm{d}\Gamma \\ &+ \int_{\Gamma_S} T_{ijk}(\mathbf{x}, \mathbf{x}') \sum_{\alpha} u_i^{\alpha}(M^{\alpha}_{,l}(\xi))'\, \rho_l L(\xi)\, \mathrm{d}\Gamma \end{aligned} \tag{15}$$

where the subscript ', l' denotes differentiation with respect to ρ_l.

The last term on the right-hand side of equation (15) is hypersingular. All integrals contained within the $\hat{c}_{iljk}$ term and the second term on the right-hand side of equation (15) are strongly singular. The integration for these terms is based upon the singularity subtraction technique using series expansions as employed by Mi and Aliabadi[5] for the evaluation of the traction BIE in the dual boundary element method. If equation (15) is written in a simplified form, such that

$$\hat{c}_{iljk}\, u'_{i,l} = I_{jk} \tag{16}$$

then via Hooke's Law the stresses at the source point can be obtained using the expression,

$$\sigma'_{i,l} = E_{ilpq}\, u'_{p,q} = E_{ilpq}\, \hat{c}^{-1}_{jkpq}\, I_{jk} \tag{17}$$

and finally the tractions are given by

$$t_i^m = n_l^m\, \sigma'_{i,l} = n_l^m\, E_{ilpq}\, \hat{c}^{-1}_{jkpq}\, I_{jk} \tag{18}$$

where index m refers to a quantity evaluated on element m at the source point. Immediately apparent from this equation is that for source points located at elements whose orientations are different (e.g. corners or edges), more than one equation will exist. Choosing only one of these equations would lead to an incomplete representation of the problem. To produce a unique TBIE these equations are summed in a weighted manner such that their fractional contribution is proportional to the angle subtended at the source point by the boundary element.[10] Thus, finally the TBIE can be written as,

$$\sum_m \phi^m t_i^m = \sum_m \phi^m n_l^m E_{ilpq} \hat{c}_{jkpq}^{-1} I_{jk} \tag{19}$$

or

$$\sum_m \phi^m t_i^m = Z_{ijk} I_{jk} \tag{20}$$

where

$$Z_{ijk} = \sum_m \phi^m n_l^m E_{ilpq} \hat{c}_{jkpq}^{-1} \tag{21}$$

4.2. Dual boundary element formulation

In the case of crack problems the DDBIE includes two extra free terms due to the proximity of the opposite surface. Following the procedure described in Reference 10 the DDBIE can be cast in the form

$$\sum_m \phi^m (t_i^{(m)+} - t_i^{(m)-}) + Z_{ijk} a_{pqjk} (u_{p,q}^+ + u_{p,q}^-) = Z_{ijk} \hat{I}_{jk}, \tag{22}$$

where

$$Z_{ijk} = \sum_m \phi^m n_l^{(m)+} E_{ilpq} s_{jkpq}^{-1} \tag{23}$$

Taking the summation in equation (22) only over crack elements ensures the presence of a strong crack pressure term, particularly important for problems where the crack surfaces are loaded. The displacement derivative terms in equation (22) are calculated using information from all elements containing the source point.

5. NUMERICAL RESULTS

In all the applications considered in this section, the localizing function utilized in equations (11) and (14) was taken to be the shape function associated with the source point (M'), this having the desired property of being equal to one at the source point and zero at element edges not containing the source point.

5.1. Earthquake control

The problem of interest is that of injecting water into an earthquake fault which is done in order to introduce controlled slip so that the accumulated strain energy can be carefully released and a potential earthquake averted. The fault is modelled as a rectangular crack under the action of shear stress as shown in Figure 2.

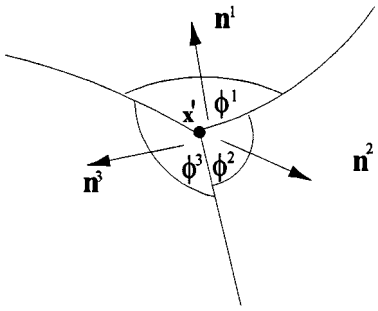

Figure 1. Normals and angles subtended at a corner point

P_o and P_f are the natural tectonic and frictional stresses, respectively. P_w is the frictional stress over the water-weakened area. The idea is to reduce the sliding mode stress intensity factor (K_{II}) at point Q to zero. This can be achieved by considering the problem as the superposition of two simpler problems, which are

(i) the whole crack under shear $P_f - P_o$
(ii) the water weakened area under shear $P_w - P_f$.

Results for two geometric configurations ($b/a = 2$, $b_w/a = 1$ and $b/a = 3$, $b_w/a = 1$) are shown in Figures 3 and 4, respectively. Since the geometry is regular and the crack surfaces are meshed with 8-noded quadrilateral elements a regular mesh is produced. This means quarter point elements can be employed along the crack front to model the square root variation of the displacement with distance from the crack front. Quarter point elements are known to produce unsatisfactory results with irregular meshes since certain geometrical conditions (see Refference 18) may not be satisfied. The stress intensity factors are evaluated using a formula based upon the extrapolation of the one-point values. This formula can be written for quarter point elements as

$$K_{II}^{Q} = \frac{E}{12(1-v^2)} \sqrt{\left(\frac{\pi}{2l}\right)} (8\Delta u^{Q'} - \Delta u^{Q''}) \tag{24}$$

where Δu refers to the crack opening displacement normal to the crack face, K_{II} denotes the sliding mode stress intensity factor (i.e. Mode II), and l is the length of the element side perpendicular to the crack front direction. On this element side, Q is the node lying on the crack front, Q' is the quarter point node and Q'' is the remaining node.

In order to arrest crack growth

$$K_{II}^{(i)} + K_{II}^{(ii)} = 0 \tag{25}$$

or

$$K_{II}^{(i)} = -K_{II}^{(ii)} \tag{26}$$

where the superscript refer to the two loading cases (i) and (ii) defined above and K_I denote the opening mode stress intensity factor (i.e. Mode I).

Reverting to normalized stress intensity factors gives

$$\hat{K}_{II}^{(i)}(P_f - P_o)\sqrt{(\pi a)} = -\hat{K}_{II}^{(ii)}(P_w - P_f)\sqrt{(\pi a)} \tag{27}$$

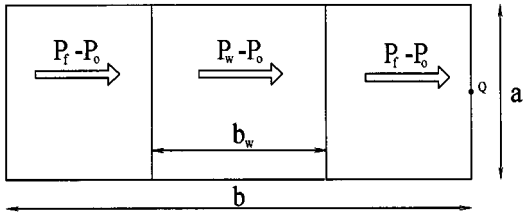

Figure 2. Fault with water weakened area

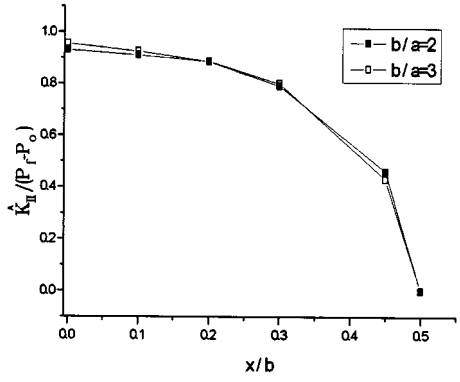

Figure 3. Full shear over crack

Table I. Stress intensity factors for earthquake control problem

b/a	$\hat{K}_{II}^{(i)}$	$\hat{K}_{II}^{(ii)}$	ω	Weaver	Error
2	0·931	0·158	5·89	5·79	1·7%
3	0·955	0·062	15·4	15·4	0·1%

so that

$$\frac{P_f - P_w}{P_o - P_f} = \frac{\hat{K}_{II}^{(i)}}{\hat{K}_{II}^{(ii)}} = \omega \tag{28}$$

Weaver[19] has obtained a relationship between ω and the crack geometry, using a displacement discontinuity technique, for fixed stresses over a range of geometries. Comparisons with the results in Reference 19 are made in Table I for the two configurations studied.

Results obtained using the DBEM compare favourably with those of Weaver especially in the second case.

5.2. *Hydraulic fracture*

Hydraulic fracture is the process of fluid-induced fracture in layers of the earth's crust for stimulating oil and gas production from depleted or low-permeability formations. The petroleum

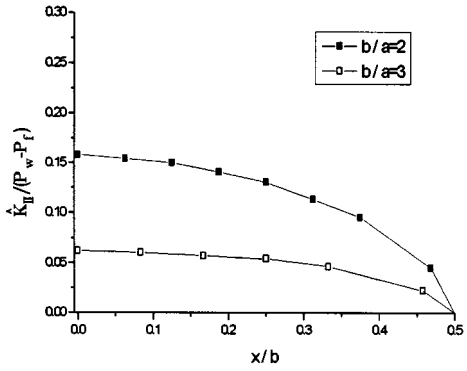

Figure 4. Partial shear over weakened area

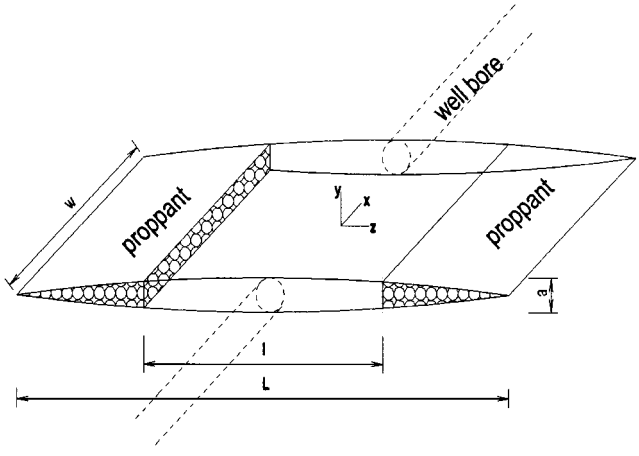

Figure 5. Hydraulic fracture with residual proppant

industry induces hydraulic fracture in oil wells by the injection of fluid into the well at high pressure. Suspended particles in the high-pressure fluid are deposited after the fluid has drained, leaving the crack propped open (see Figure 5) and so increasing the effective wellbore radius (the area available for drainage) and thus the rate at which oil is recovered.

Opened fractures can be still modelled as cracks because the width (typically 1 cm) is usually negligible compared to the length (typically 30–300 m) and the height (3–30 m). In order to model interaction between crack surfaces that are propped open spring constraints are introduced between opposing nodes on the crack surface. The stiffness of these springs in the normal and shear directions are defined in terms of the elastic properties of the proppant.

In the areas of the crack which are propped opened, extra unknowns are introduced into the system of equations since neither the stresses nor the displacements caused by the proppant are unknown beforehand. Additional equations are produced by modelling the proppant as a linear elastic solid. This is done by connecting opposing nodes on the crack surfaces with springs constraints for the normal and tangential directions as depicted in Figure 6. There also exists an initial state of stress in the rock (that existed before the creation of the fracture) so that the final

stresses are given by

$$\sigma'_{\mathrm{n}} = \sigma^0_{\mathrm{n}} + \Delta\sigma_{\mathrm{n}} \tag{29}$$

and

$$\sigma'_{\mathrm{s}} = \sigma^0_{\mathrm{s}} + \Delta\sigma_{\mathrm{s}} \tag{30}$$

where the superscript (^{0}) indicates the initial state, and Δ indicates the induced values. The final state of stress in the springs is then related to the change in displacement by Hooke's law, which for the normal stress is given by

$$\sigma'_{\mathrm{n}} = -k_{\mathrm{n}}\Delta u_{\mathrm{n}} \tag{31}$$

and for the shear stress by

$$\sigma'_{\mathrm{s}} = -k_{\mathrm{s}}\Delta u_{\mathrm{s}} \tag{32}$$

where k_{n} and k_{s} are the normal and shear stiffnesses, and Δu_{n} and Δu_{s} are the corresponding displacements. The stiffnesses are defined in terms of the elastic properties of the proppant by

$$k_{\mathrm{n}} = \frac{E}{a} \tag{33}$$

and

$$k_{\mathrm{s}} = \frac{E_{\mathrm{prop}}}{2(1+\upsilon_{\mathrm{prop}})a} \tag{34}$$

where a is the crack thickness, E and E_{prop} are Young's modulus of the rock material and proppant, respectively, and υ_{prop} is Poisson's ratio for the proppant.

The reference state is the undeformed proppant shape and not the undeformed fracture shape, therefore

$$\Delta u_{\mathrm{n}} = u'_{\mathrm{n}} \tag{35}$$

$$\Delta u_{\mathrm{s}} = u'_{\mathrm{s}} \tag{36}$$

Then the relationships between tractions and displacements of nodes on the upper (denoted by $+$) and the lower surface (denoted by $-$) are given by

$$t^+_{\mathrm{n}} + k_{\mathrm{n}}(u^+_{\mathrm{n}} - u^-_{\mathrm{n}}) = -(t^+_{\mathrm{n}})^0 \tag{37}$$

$$t^+_{\mathrm{s}} + k_{\mathrm{s}}(u^+_{\mathrm{s}} - u^-_{\mathrm{s}}) = -(t^+_{\mathrm{s}})^0 \tag{38}$$

$$t^+_{\mathrm{n}} + t^-_{\mathrm{n}} = -(t^+_{\mathrm{n}})^{\mathrm{o}} - (t^-_{\mathrm{n}})^0 \tag{39}$$

$$t^+_{\mathrm{s}} + t^-_{\mathrm{s}} = -(t^+_{\mathrm{s}})^{\mathrm{o}} - (t^-_{\mathrm{s}})^0 \tag{40}$$

where the Δ has been dropped for convenience and the known quantities have been moved to the right hand side. Conventionally, the BEM matrix system is assembled as

$$\mathbf{Hu} = \mathbf{Gt} \tag{41}$$

and with all unknowns transferred to the right-hand side and all knowns to the left-hand side, the system becomes

$$\mathbf{Ax} = \mathbf{B} \tag{42}$$

When the spring constraints are introduced the matrix system takes the form

$$\left(\begin{array}{c|cccc} \mathbf{A}^{\mathrm{NC}} & \mathbf{H}^{C+} & \mathbf{H}^{C-} & \mathbf{G}^{C+} & \mathbf{G}^{C-} \\ \hline 0 & \multicolumn{4}{c}{D^{\mathrm{C}}} \end{array}\right)\left(\begin{array}{c} \mathbf{x}^{\mathrm{NC}} \\ \hline \mathbf{u}^{C+} \\ \mathbf{u}^{C-} \\ \mathbf{t}^{C+} \\ \mathbf{t}^{C-} \end{array}\right)=\left(\begin{array}{c} \mathbf{B}^{\mathrm{NC}} \\ \hline \mathbf{B}^{\mathrm{C}} \end{array}\right) \tag{43}$$

where the superscripts NC, $C+$, $C-$ refer to the non-contact region , the upper crack surface contact nodes, and the lower crack surface nodes, respectively. The D^C area of the matrix contains the unknowns (i.e., the left-hand side) of the constraint equations (37)–(40) and the B^{C} area contains the known quantities (i.e, the right-hand side) of these equations. For example, when a single pair of contact nodes is considered,

$$D^{\mathrm{C}}=\begin{pmatrix} k_n & -k_n & 1 & 0 \\ k_s & -k_s & 1 & 0 \\ 0 & 0 & 1 & 1 \\ 0 & 0 & 1 & 1 \end{pmatrix} \tag{44}$$

and correspondingly,

$$B^{\mathrm{C}}=\begin{pmatrix} -(t_{\mathrm{n}}^{+})^{0} & \\ -(t_{\mathrm{s}}^{+})^{0} & \\ -(t_{\mathrm{n}}^{+})^{0} & -(t_{\mathrm{n}}^{-})^{0} \\ -(t_{\mathrm{s}}^{+})^{0} & -(t_{\mathrm{s}}^{-})^{0} \end{pmatrix}. \tag{45}$$

When nodes lie the on the interface of the contact/non-contact region some thought has to be given to the assembly of the matrix. Only the relevant elemental components of the G matrix corresponding to those elements with known tractions (i.e., in the non-contact region) should be included in the $\mathbf{A}^{\mathrm{NC}}$ region of the matrix. The remaining elemental components combine to give a unique traction so that equations (37)–(40) take the form

$$t_{\mathrm{n}}^{C+}+k_{\mathrm{n}}(u_{\mathrm{n}}^{+}-u_{\mathrm{n}}^{-})=-(t_{\mathrm{n}}^{C+})^{0} \tag{46}$$

$$t_{\mathrm{s}}^{C+}+k_{\mathrm{s}}(u_{\mathrm{s}}^{+}-u_{\mathrm{s}}^{-})=-(t_{\mathrm{s}}^{C+})^{0} \tag{47}$$

$$t_{\mathrm{n}}^{C+}+t_{\mathrm{n}}^{C-}=-(t_{\mathrm{n}}^{C+})^{0}-(t_{\mathrm{n}}^{C-})^{0} \tag{48}$$

$$t_{\mathrm{s}}^{C+}+t_{\mathrm{s}}^{C-}=-(t_{\mathrm{s}}^{C+})^{0}-(t_{\mathrm{s}}^{C-})^{0} \tag{49}$$

In the first configuration studied the geometric parameters were such that $a=0{\cdot}5$ m, $l=240$ m, $L/l=5$, and $w=L$ and the far-field compressive stresses were such that $\sigma_{yy}=1500$ Pa with all other component of the stress tensor being zero. The elastic properties are given such that $E=2{\cdot}3\times10^{6}$ Pa, $\nu=0{\cdot}15$, $E_{\mathrm{prop}}=0{\cdot}35\times10^{6}$ Pa and $\upsilon_{\mathrm{prop}}=0{\cdot}2$. Figure 7 shows the profile cross section at $x=0{\cdot}0$ where plain strain conditions are assumed to hold. Results converge satisfactorily and are in general agreement with those obtained by Asgian[20] who employed a two-dimensional displacement discontinuity technique utilising constants elements.

Next, the effect of varying the ratio of Young's moduli was studied as shown in Figure 8 where $R=E_{\mathrm{prop}}/E$. The amount of proppant deformation can be seen to decrease as R is increased. The profile converges towards the analytic solution ($R=\infty$) which can be derived from that of a pressurized crack in an infinite body.

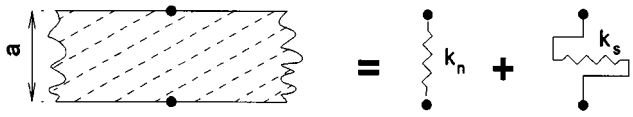

Figure 6. Modelling of proppant by elastic springs

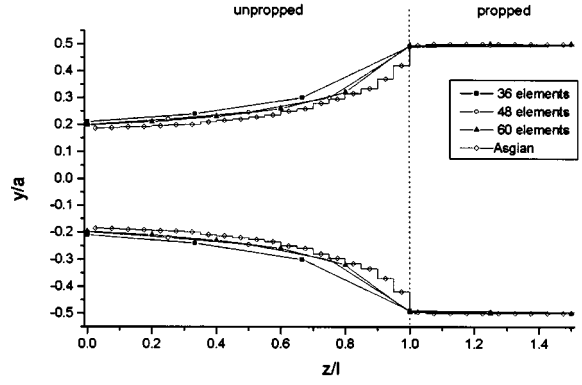

Figure 7. Propped crack profile

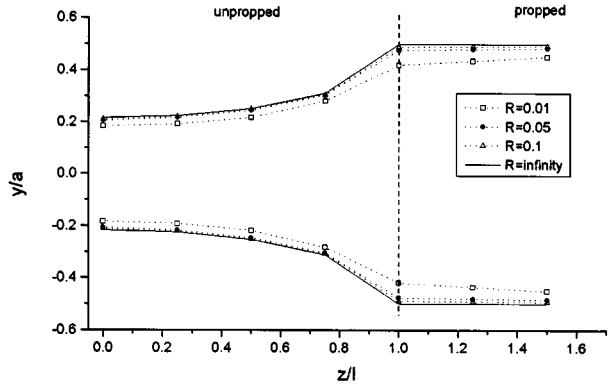

Figure 8. Effect of rock/proppant modulus ratio on crack profile

5.3. *Seam extraction*

In the problem under consideration the seam is sufficiently far from the earth's surface that the rock mass surrounding it can be assumed to be linearly elastic. The springs constraints developed in the last section are used to investigate the closure and stresses during the extraction of an ore seam. An additional complication in this application is that normal and shear directions on the seam do not correspond to the global directions in which the boundary integral equations are formulated. With reference to Figure 9, which shows the geometry and meshing of this problem, the tractions and displacements in global system are related to those in the seam co-ordinates by

$$\mathbf{t}' = \mathbf{R}\mathbf{t} \tag{50}$$

$$\mathbf{u}' = \mathbf{R}\mathbf{u} \tag{51}$$

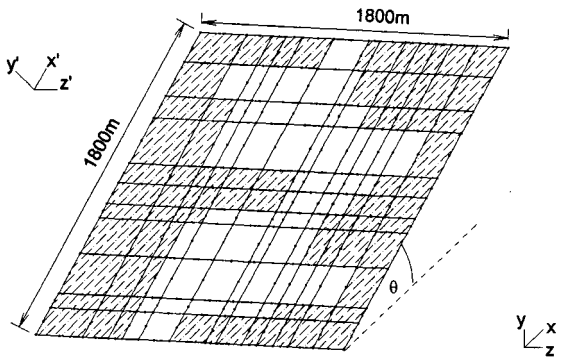

Figure 9. Mesh and geometry of a partially extracted seam

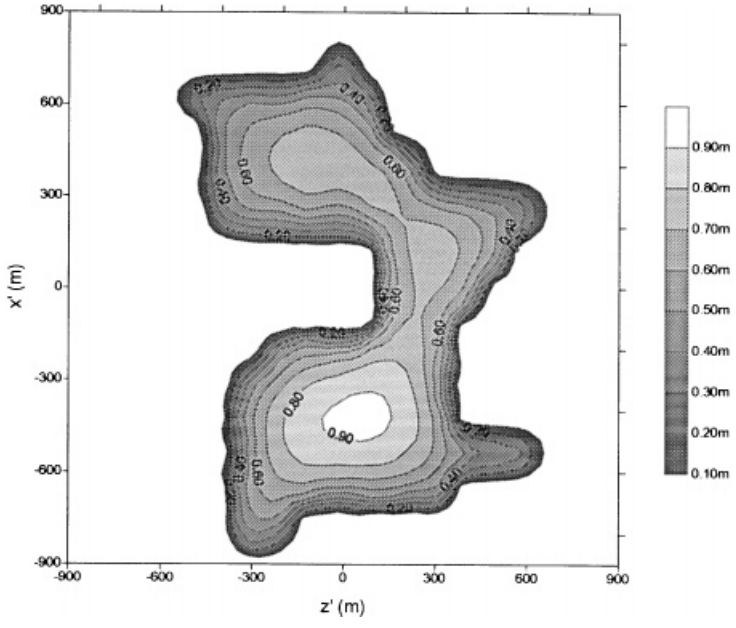

Figure 10. Contour plot of closure

where **R** is the rotation matrix given by,

$$\mathbf{R} = \begin{pmatrix} \cos\theta & \sin\theta & 0 \\ \cos\theta & -\sin\theta & 0 \\ 0 & 0 & 1 \end{pmatrix} \tag{52}$$

These can then be substituted into equations (37)–(40) or equations (46)–(49) to obtain the D^{c} component of the system matrix and the B^{C} component of the right-hand side vector.

The seam dimensions and parameters are taken from Reference 2, and are such that the seam can be approximated as an ore-filled crack. Figure 9 shows the geometry and meshing of this problem. The unmined areas (indicated by hatching in Figure 9) are modelled using the spring constraints developed in the previous section. In this example, the proppant is in fact the rock material, so only the elastic properties of this ($E = 7{\cdot}0 \times 10^4$ Pa, $\nu = 0{\cdot}2$) need to be specified. The

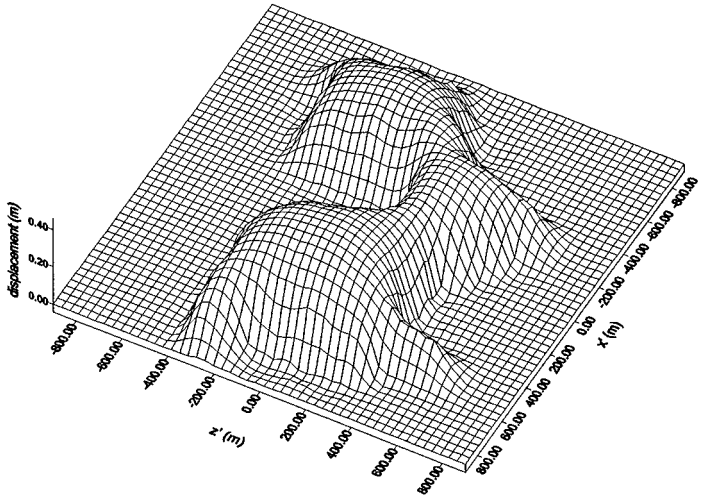

Figure 11. Surface plot of deformed seam floor

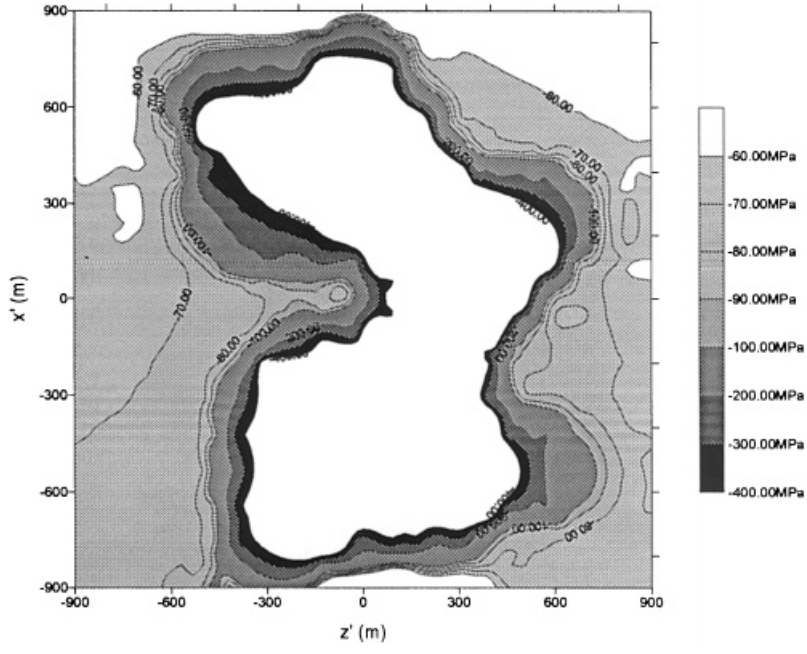

Figure 12. Contour plot of normal stresses in partially extracted seam

y-axis is in the vertical direction with respect to the earth's surface. The angle θ is taken as 30°, the thickness of the seam as 1 m and the depth of the centre of the seam as 2650 m. The initial stresses are given as

$$\sigma_{xx} = -D \times 0{\cdot}027 \times 10^6 \text{ Pa}$$

$$\sigma_{yy} = \sigma_{xx}/2 \text{ Pa}$$

$$\sigma_{zz} = \sigma_{xx}/2 \text{ Pa}$$

where D is the depth. The displacement of the lower surface is shown in Figure 10 and the closure in Figure 11. A point of interest from the second figure is that, in a limited area, there is the possibility of total closure. The model does not prevent the overlap of the footwall (floor) and hanging wall (roof) of the seam, and if this area was of a greater extent an incremental loading procedure, and some consideration of the type of contact, would be necessary. However, since this area is negligible in this example the method developed was sufficiently sophisticated. Figure 12 shows the normal stresses in the seam plain (σ'_{yy}) and as expected they are highest at the edges of the unmined/mined areas.

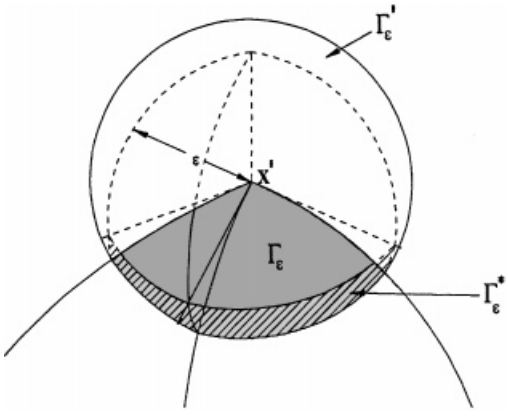

Figure 13. Augmented surface for limiting process

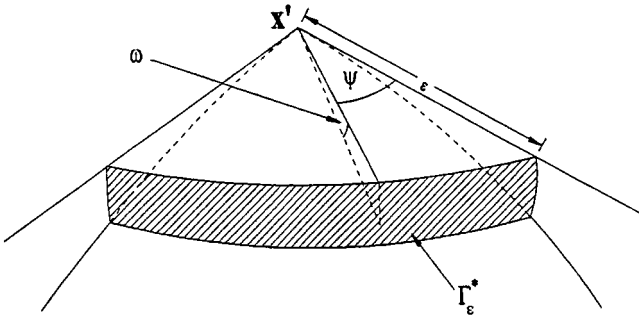

Figure 14. Coordinate system for surface Γ_ε^*

6. CONCLUSION

A dual boundary element method employing purely continuous elements has been developed for the analysis of fracture or fracture-like problems in three dimensions. An example from earthquake control theory was used to verify the technique for partially loaded crack surfaces. The method was then extended to deal with contact between crack surfaces by the incorporation of spring constraints between opposing nodes on the upper and lower crack surfaces nodes. This allowed two further applications to be studied, one from hydraulic fracture and the other involving extraction of an ore seam. Results from theses studies demonstrate the efficiency of the technique for the analysis of three-dimensional fractures in geomechanics.

APPENDIX I

The Kelvin fundamental solutions for a three-dimensional isotropic solid are given by

$$U_{ij}(\mathbf{x}, \mathbf{x}') = \frac{1+v}{8\pi(1-v)Er}\{(3-4v)\delta_{ij} + r_{,i}r_{,j}\} \tag{53}$$

$$T_{ij}(\mathbf{x}, \mathbf{x}') = \frac{-1}{8\pi(1-v)r^2}\{[(1-2v)\delta_{ij} + 3r_{,i}r_{,j}]r_{,k}n_{,k} + (1-2v)[r_{,i}n_{,j} - r_{,j}n_{,i}]\} \tag{54}$$

where $r_i = x_i - x'_i$, $r_{,i} = \partial r/\partial x_i$ and n is the outward normal to the surface at the point $\mathbf{x}$. They represent the i-components of displacement and traction at the point $\mathbf{x}$ due to a point force acting in the j-direction at the point $\mathbf{x}'$.

Differentiating equations (53) and (54) with respect to $\mathbf{x}'$ gives

$$U_{ijk}(\mathbf{x}, \mathbf{x}') = \frac{1+v}{8\pi(1-v)Er^2}\{(3-4v)\delta_{ij}r_{,k} + 3r_{,i}r_{,j}r_{,k} - \delta_{jk}r_{,i} - \delta_{ki}r_{,j}\} \tag{55}$$

$$\begin{aligned} T_{ijk}(\mathbf{x}, \mathbf{x}') = \frac{-1}{8\pi(1-v)r^3}\{&[(1-2v)\delta_{ij}r_{,k} + 3r_{,i}r_{,j}]n_k \\ &- (1-2v)[\delta_{jk} - 3r_{,j}r_{,k}]n_i \\ &+ (1-2v)[\delta_{ki} - 3r_{,k}r_{,i}]n_j \\ &+ [3\delta_{jk}r_{,i} + 3\delta_{ki}r_{,j} - 3(1-2v)\delta_{ij}r_{,k} - 15r_{,i}r_{,j}r_{,k}]r_{,l}n_{,l,k}\} \end{aligned} \tag{56}$$

APPENDIX II

The boundary integral equation (3) is derived by considering the limiting case of equation (2) as the source point approaches to the boundary. The processes is similar to the conventional displacement integral equation (see Reference 21), however, for this analysis the augmented spherical surface (radius ε) is considered to be composed of two constituent surfaces Γ'_ε and Γ^*_ε. The surface Γ^*_ε is the component of the spherical surface confined by the tangents plane at $\mathbf{x}'$ and the original surface Γ. The surface Γ'_ε is the remaining hemi-spherical component. These surfaces are shown for fully general point in Figure 13 and its clear that Γ^*_ε exist only by virtue of the surface curvature at $\mathbf{x}'$. In the limit $\varepsilon \to 0$ the augmented boundary composed of $\Gamma - \Gamma_\varepsilon +$

$\Gamma'_\varepsilon + \Gamma^*_\varepsilon$ tends towards the actual boundary Γ. Define the integral,

$$I_\Gamma = \lim_{\varepsilon \to 0} \left[\int_\Gamma \{T_{ij,k}(\mathbf{x}', \mathbf{x}) u_i(\mathbf{x}) - U_{ij,k}(\mathbf{x}', \mathbf{x}) t_i(\mathbf{x})\} \, \mathrm{d}\Gamma(\mathbf{x}) \right]$$
$$= I_{\Gamma - \Gamma_\varepsilon} + I_{\Gamma'_\varepsilon} + I_{\Gamma^*_\varepsilon} \tag{57}$$

where $\mathbf{x}' \in \Omega$, $\mathbf{x} \in \Gamma$, and $\Gamma_{\Gamma - \Gamma_\varepsilon}$, $I_{\Gamma'_\varepsilon}$ and $I_{\Gamma^*_\varepsilon}$ are the limits of the integrals over the component surface. Next, the form of these integrals are considered in more detail.

II.1. The surface Γ'_ε

The integration over this surface can be written as

$$I_{\Gamma'_\varepsilon} = \lim_{\varepsilon \to 0} \left[\int_{\Gamma'_\varepsilon} \{T_{ij,k}(\mathbf{x}', \mathbf{x}) u_i(\mathbf{x}) - U_{ij,k}(\mathbf{x}', \mathbf{x}) t_i(\mathbf{x})\} \, \mathrm{d}\Gamma(\mathbf{x}) \right] \tag{58}$$

Since we are integrating over a sphere the differential area is given by

$$\mathrm{d}\Gamma(\mathbf{x}) = \varepsilon^2 \sin\theta \, \mathrm{d}\theta \, \mathrm{d}\phi \tag{59}$$

and also the outward pointing normal n is related to the relative position vector of the source and field points by

$$\mathbf{r} = \mathbf{x} - \mathbf{x}' = \varepsilon \mathbf{n} \tag{60}$$

On a continuous part of the surface near to the surface point, the displacement should be continuous and differentiable, i.e. should take the form,

$$u_i(\mathbf{x}) = u'_i + u'_{i,j} r_j + O(r^2) \tag{61}$$

where the superscript $'$ denotes evaluation at the source point. Combining equations (60) with (61), one obtains

$$u_i(\mathbf{x}) = u'_i + \varepsilon n_k u'_{i,k} + O(\varepsilon^2) \tag{62}$$

When equation (60) is substituted into the kernel expressions $U_{ij,k}$ and $T_{ij,k}$, they take the form

$$U_{ij,k}(\mathbf{x}', \mathbf{x}) = \varepsilon^{-2} \hat{U}_{ijk}(n) \tag{63}$$

$$T_{ij,k}(\mathbf{x}', \mathbf{x}) = \varepsilon^{-3} \hat{T}_{ij,k}(n) \tag{64}$$

where

$$\hat{U}_{ijk}(n) = \frac{(1+\nu)}{8\pi(1-\nu)E} [3n_i n_j n_k + (3-4\nu)\delta_{ij} n_k - \delta_{ki} n_j - \delta_{jk} n_i] \tag{65}$$

$$\hat{T}_{ij,k}(n) = \frac{-1}{4\pi(1-\nu)} [6n_i n_j n_k + (1-2\nu)\delta_{ij} n_k - (1+\nu)\delta_{ik} n_j - (2-\nu)\delta_{kj} n_i] \tag{66}$$

Substituting expressions (59), (61), (63) and (64) into equation (58), and applying Hooke's law ($t'_p = n'_q E_{pqil} u'_{i,l}$) gives

$$I_{\Gamma'_\varepsilon} = \lim_{\varepsilon \to 0} [\varepsilon^{-1} \bar{B}_{ijk}(\mathbf{x}') u'_i] + c_{iljk}(\mathbf{x}') u'_{i,l} + O(\varepsilon) \tag{67}$$

where

$$\bar{B}_{ijk}(\mathbf{x}') = \int_{\Gamma'_\varepsilon} \hat{T}_{ijk}(\mathbf{n}) \sin\theta \, \mathrm{d}\theta \, \mathrm{d}\phi \tag{68}$$

and

$$c_{iljk}(\mathbf{x}') = \int_{\Gamma'_\varepsilon} [\hat{T}_{ijk}(\mathbf{n})\mathbf{n}'_l - \hat{U}_{pjk}(\mathbf{n}) n'_q E_{pqil}] \sin\theta \, \mathrm{d}\theta \, \mathrm{d}\phi \tag{69}$$

II.2. The Surface $\Gamma - \Gamma_e$

In order to evaluate the integral expression,

$$I_{\Gamma-\Gamma_\varepsilon} = \lim_{\varepsilon\to 0} \int_{\Gamma-\Gamma_\varepsilon} \{T_{ijk}(\mathbf{x}', \mathbf{x}) u_i(\mathbf{x}) - U_{ijk}(\mathbf{x}', \mathbf{x}) t_i(\mathbf{x})\} \, \mathrm{d}\Gamma(\mathbf{x}) \tag{70}$$

it is necessary to expand the kernels in terms of the polar co-ordinates (ρ, ψ) defined on the tangent plane centered at $\mathbf{x}'$. The expanded kernel take the form

$$\begin{aligned} T_{ijk}(\mathbf{x}', \mathbf{x}) &= \rho^{-3} T^{(3)}_{ijk}(\psi) + \rho^{-2} T^{(2)}_{ijk}(\psi) + O(\rho^{-1}) \\ U_{ijk}(\mathbf{x}', \mathbf{x}) &= \rho^{-2} U^{(2)}_{ijk}(\psi) + O(\rho^{-1}) \end{aligned} \tag{71}$$

On this surface $r_j = \rho_j + O(\rho^2)$ and since $\rho_j = \rho_{,j}\rho$, equation (62) takes the form,

$$u_i(\mathbf{x}) = u'_i + u'_{i,j}\rho_{,j}\rho + O(\rho^2) \tag{72}$$

The differential area in this case is given by

$$\mathrm{d}\Gamma(\mathbf{x}) = \rho \, \mathrm{d}\rho \, \mathrm{d}\psi \tag{73}$$

Substituting equations (71)–(73) into equation (70) gives, after some simplifying,

$$\begin{aligned} I_{\Gamma-\Gamma_\varepsilon} = \lim_{\varepsilon\to 0} [\varepsilon^{-1} B_{ijk}(\mathbf{x}') u'_j + \log\varepsilon \{\alpha_{ijk}(\mathbf{x}') u'_j + \beta_{iljk}(\mathbf{x}') u'_{i,l} + \gamma_{jik}(x') t'_i\}] \\ + \int_{\Gamma-\Gamma_c} = T_{ijk}(\mathbf{x}', \mathbf{x}) u_i(\mathbf{x}) \, \mathrm{d}\Gamma(\mathbf{x}) - \int_{\Gamma-\Gamma_c} - U_{ijk}(\mathbf{x}', \mathbf{x}) t_i(\mathbf{x}) \, \mathrm{d}\Gamma(\mathbf{x}) \end{aligned} \tag{74}$$

where the Cauchy and Hadamard Principal Value notation, and

$$B_{ijk}(\mathbf{x}') = -\int_{\Gamma_\varepsilon} T^{(3)}_{ijk}(\psi) \, \mathrm{d}\psi, \; \alpha_{ijk}(\mathbf{x}') = \int_{\Gamma_\varepsilon} T^{(2)}_{ijk}(\psi) \, \mathrm{d}\psi, \; \mathrm{B}_{ilk}(\mathbf{x}') = \int_{\Gamma_\varepsilon} T^{(3)}_{ijk}(\psi)\rho_j \, \mathrm{d}\psi \tag{75}$$

and

$$\gamma_{ijk}(\mathbf{x}') = -\int_{\Gamma_\varepsilon} U^{(2)}_{ijk}(\psi) \, \mathrm{d}\psi \tag{76}$$

where $S_\varepsilon = \Gamma'_\varepsilon \cap \Gamma^*_\varepsilon$.

II.3. The Surface Γ_ε^*

In order to evaluate to integral expression,

$$I_{\Gamma_\varepsilon} = \lim_{\varepsilon \to 0} \int_{\Gamma_\varepsilon^*} \{T_{ijk}(\mathbf{x}', \mathbf{x}) u_i(\mathbf{x}) - U_{ijk}(\mathbf{x}', \mathbf{x}) t_i(\mathbf{x})\} \, \mathrm{d}\Gamma(\mathbf{x}) \tag{77}$$

an additional off-plane co-ordinate is introduced as indicated in Figure 14. The differential area in this case is given by

$$\mathrm{d}\Gamma = \varepsilon^2 \cos\omega \, \mathrm{d}\omega \, \mathrm{d}\psi \tag{78}$$

and the limits of integration for a particular m as $\psi_1^m \leqslant \psi \leqslant \psi_2^m$; $0 \leqslant \omega \leqslant \omega_2^m$. With reference to Figure 14 it can be shown that

$$\tan \omega_2^m = \frac{\frac{1}{2}\varepsilon^2 \kappa^m(\psi)}{\varepsilon} = \frac{\varepsilon \kappa^m(\psi)}{2} \tag{79}$$

where $\kappa^m(\psi)$ is the curvature of element m. Since the average angle small, the approximation $\omega_2^m = \tan^{-1}(\varepsilon\kappa^m(\psi)/2) \simeq \varepsilon\kappa^m(\psi)/2$ can be employed. Substituting the kernels given in expression (63) and (64) together with the expression for the differential area equation (78), into equation (79), one finds

$$I_{\Gamma_\varepsilon^*} = \sum_m^M \int_{\psi_1^m}^{\psi_2^m} \left[\lim_{\varepsilon \to 0} \frac{1}{2} \int_0^{1/2\varepsilon\kappa^m(\psi)} (\hat{T}_{ijk}(\psi, \omega) u_i' + O(\varepsilon)) \cos\omega \, \mathrm{d}\omega \right] \mathrm{d}\psi \tag{80}$$

where M is the total number of elements surrounding the source point. The limit within the square brackets is of the form,

$$\lim_{\varepsilon \to 0} \frac{1}{\varepsilon} \int_0^{1/2\varepsilon\kappa^m(\psi)} f(\psi, \omega) \, \mathrm{d}\omega \tag{81}$$

which, according to mean limit value theorem, is equivalent to

$$\lim_{\varepsilon \to 0} \left\{ \frac{1}{\varepsilon} f(\psi, 0) \left[\frac{1}{2} \varepsilon \kappa^m(\psi) - 0 \right] \right\} \tag{82}$$

and this simplifies to $1/2\kappa^m(\psi) f(\psi, 0)$. Finally (79) can be expressed as,

$$\begin{aligned} I_{\Gamma_\varepsilon^*} &= \sum_m^M \int_{\psi_1^m}^{\psi_2^m} \frac{1}{2} \kappa^m \hat{T}_{ijk}(\psi, \omega) u_i' \, \mathrm{d}\psi + O(\varepsilon) \\ &= d_{ijk}(\mathbf{x}') u_i' + O(\varepsilon), \end{aligned} \tag{83}$$

where d_{ijk} term is $O(1)$ and given by

$$d_{ijk}(\mathbf{x}') = \frac{1}{2} \sum_m^M \int_{\psi_1^m}^{\psi_2^m} \kappa^{(m)} \hat{T}_{ijk}(\psi, 0) \, \mathrm{d}\psi$$

REFERENCES

1. G. Manolis and T. Davies, *Boundary Element Techniques in Geomechanics*, Computational Mechanics Publications, Southampton, 1993.
2. S. Crouch and A. Starfield, *Boundary Element Methods in Solid Mechanics*, George Allen and Unwin, London, 1983.
3. L. J. Gray, L. F. Martha and A. R. Ingraffea, 'Hypersingular integrals in boundary analysis', *Int. J. Numer. Meth. Engng*., **29,** 1135–1158 (1990).
4. A. Portela, M. H. Aliabadi and D. P. Rooke, 'The dual boundary element method: effective implementation for crack problems', *Int. J. Num. Meth. Engng*., **33,** 1269–1287 (1992).
5. Y. Mi and M. H. Aliabadi, 'Dual boundary element method for three dimensional fracture mechanics analysis', *Engng. Anal. Boundary Elements*, **10**(2), 161–171 (1992).
6. L. F. Martha, L. J. Gray and A. R. Ingraffea, 'Three-dimensional fracture simulation element fracture with a single domain, direct boundary element formulation', *Int. J. Numer. Meth. Engng*., **35,** (1992).
7. M. H. Aliabadi, 'Boundary element formulations in fracture mechanics', *Appl. Mech. Rev*., **50**(2), 83–96 (1997).
8. M. H. Aliabadi, 'A new generation of boundary element formulations for fracture mechanics', *Int. J. Fracture*, **42,** 91–125 (1998).
9. A. Portela and M. H. Aliabadi, 'Dual boundary element analysis of crack growth', Advances in Boundary Element Formulations, Chapter 1, Computational Mechanics Publications, Southampton, 1993.
10. A. Young, 'A single-domain boundary element method for 3-D elastostatic crack analysis using continuous elements', *Int. J. Numer. Meth. Engng*., **39,** 1265–1293 (1996).
11. A. Wilde, and M. H. Aliabadi, 'Dual boundary element method for geomechanics problems using continuous elements', in C. A. Brebbia, J. Martinez and M. H. Aliabadi (eds), *Boundary Elements XVIII*, Comput. Mech. Publ. Southampton, pp. 449–464
12. A. Wilde and M. H. Aliabadi, 'Direct evaluation of boundary stresses in the 3-D BEM of Elastostatics', *Commun. Numer. Meth. Engng*., submitted.
13. M. Guiggiani, 'Hypersingular boundary integral equations have an additional free term', *Comput. Mech*., **16,** 245–248 (1995).
14. V. Mantic and F. Paris, 'Existence and evaluation of the two free terms in the hypersingular boundary integral equation of potential theory', *Engng. Anal. Boundary Elements*, **16**(3)**,** 253–260 (19995).
15. T. Cruse and J. Richardson, 'Non-singular somigliana stress identities in elasticity', *Int. J. Numer. Meth. Engng*., **39,** 3273–3304 (1996).
16. P. Martin and F. Rizzo, 'Hypersingular Integrals: how smooth must the density be?', *Int. J. Numer. Meth. Engng*., **39,** 687–704 (1996).
17. V. Sladek and J. Sladek, 'Regularization of hypersingular integrals in BEM formulations using various kinds of continuous elements', *Engng. Anal. Boundary Elements*, **17,** 5–18 (1996).
18. W. H. Gerstle, 'Finite and boundary element modelling of crack propagation in two and three dimensions using interactive computer graphics', *Ph.D. Thesis*, Cornell University, Ithaca NY USA, 1986.
19. J. Weaver, 'Three-dimensional crack analysis', *Int. J. Solids Struct*., **13,** 321–330 (1977).
20. M. I. Asgian, 'Hydraulic fracture', in G. Manolis and T. Davies (eds), *Boundary Element Techniques in Geomechanics*, Computational Mechanics Publications, Southampton, 1993, 443–477
21. M. H. Aliabadi and D. P. Rooke, *Numerical Fracture Mechanics*, Kluwer Academic Publishers, Dordrechet, 1991.

